Res. Chem. Intermed., Vol. 23, No. 8, pp. 735–753 (1997)

INTERACTION OF CO_2 WITH SMALL RUTILE CRYSTALLITES - AN EHMO STUDY

I. KAMBER
Paul Scherrer Institute,CH-5232 Villigen PSI, Switzerland

Received 10 March 1997; accepted 11 April 1997

Abstract--Several possible adsorption sites and adsorption geometries of CO_2 on small rutile fragments were studied by Extended Hückel Molecular Orbital (EHMO) calculations. The parameters for the rutile part were optimised to reproduce the experimental rutile bulk structure and were tested in several small clusters up to $[(TiO_2)_{31}(OH)_{32}]^{32-} \cdot 6H_2O$, a 175 atoms cluster. It was found that the average experimental bond legth can be reproduced with good accuracy. However the slight distortion of the TiO_6 octahedra is calculated with the wrong sign (four long and two short Ti-O bonds). The agreement for the angle $\alpha_{O\text{-}Ti\text{-}O}$ is less satisfactory. The study shows that CO_2 can adsorb on fivefold coordinated surface titanium sites as well as surface oxygen sites. This means that CO_2 can act as either Lewis base or acid. In the case of binding as a Lewis base, CO_2 can adsorb linearly forming a single Ti-OCO bond, or interact with two neighboring Ti^{4+} sites. A chelating structure forming two Ti-O bonds was found to be weakly stable at the most. When CO_2 behaves as a Lewis acid, a carbonate-like structure is formed by interaction with either terminal oxygen ions or bridging oxygen centers.

INTRODUCTION

TiO_2 has been widely used as photocatalyst for a long time by now [1-5]. It can be applied in photooxidations as well as photoreductions, often with the long term goal to use solar radiation to drive the process. Probably the only solar driven process employing TiO_2 that is at the edge of being commercialised at present is photodetoxification i.e. photooxidation of organic pollutants. On the other hand, photoreduction reactions would be excellent for the photochemical transformation and storage of solar energy by synthesising "solar fuels". They are however still far from being commercialised because they generally suffer from very low yields. Most of the efforts in the field of "solar fuel" synthesis are concerned with the photochemical water splitting. They were probably all triggered by the famous paper by Fujishima and Honda [6] that showed for the first time the photochemical splitting of water although under applied bias. Despite of the various efforts even at present the splitting of water into molecular hydrogen and oxygen is still considered as one of the "Holy Grails" in chemistry [7].

A conceptually interesting reaction for solar fuel synthesis is the photoreduction of CO_2. If performed with H_2O as reductant, oxygen and small hydrocarbon molecules [8-13] are the expected products. Up to now free oxygen has never be detected and the reaction is very inefficient, meaning that it proceeds with a low quantum yield. If this reaction would occur with a reasonable efficiency "solar fuels" could be synthesised in a closed carbon cycle. As this reaction consists of the photoreduction of CO_2 on a semiconductor with a low lying valence band thus exhibiting a potential for photooxidations, care has to be taken that the products are not reoxidised immediately. Earlier results [12,13] showed that CO_2 can be reduced at TiO_2 (Degussa P25) from the gas phase in the presence of H_2O with CO, H_2, CH_4 and traces of higher hydrocarbons as products. An important point for the understanding of this reaction is the ground state interaction of the educt CO_2 with the photocatalyst. Adsorption sites and preferential adsorption geometries can influence the reaction path and can therefore determine the observed products. The aim of this paper is to understand such an interaction on the basis of the interaction of the molecular orbitals of carbon dioxide with those of rutile. Rutile was chosen in this study solely because its unit cell consists of fewer atoms than the photochemically more active anatase. This allows for the calculation of fragments that consist of a larger number of unit cells as compared to anatase.

Quite a large number of calculations employing different methods, are already available for the rutile system. They were used to described the bulk properties [14,15], surface properties [16], adsorption properties [17-19] or defect properties [20], only to mention a few. An overview over the surface properties of rutile can be found in [21] and certain aspects also in [22] .

The structure of rutile (space group $P4_2/mnm$, $a = 4.5941$ Å, $b = 2.9589$ Å) is built from slightly distorted TiO_6 octahedra of D_{4h} symmetry with two long and four short Ti-O bonds. They form infinite linear chains of edge-sharing octahedra. The angles between the four short Ti-O bonds does deviate from the ideal case where we would expect them to be all equal to 90°. The Ti-O angles pointing to the shared edge are only 81.12°. The chains formed in this way, every other rotated by 90° around the chain axis, run in parallel forming layers. These are stacked, offset horizontally by one octahedron. The building principle is illustrated in Figure 1. Note that in this figure the crystallographic axis do not run parallel to *l* and *n*. However *m* is parallel to the *c* axis.

Generally the small TiO_2 (rutile) fragments described in this paper are fully hydroxylated. This means that they are charged and do not show low coordinated Ti atoms at the surface. They can be described by the formula:

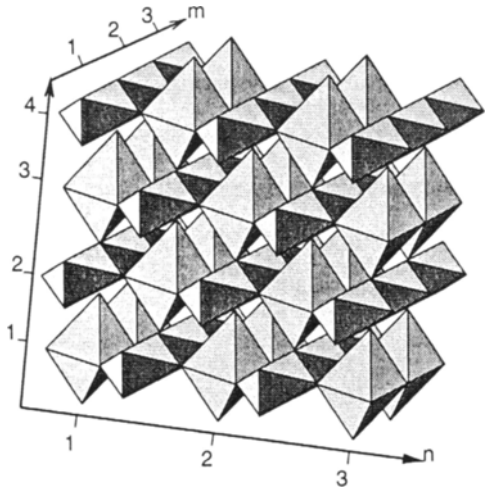

Figure 1. Definition of indices *l*, *m*, *n* and structure of small rutile fragments. Shown in the figure is a 4,3,3 fragment.

$$[(TiO_2)_x(OH)_y]^{y-} \cdot zH_2O \qquad \textbf{(1)}$$

with

$$x = l(2mn - m + n) - [\frac{l+1}{2}] \qquad \textbf{(2a)}$$

$$y = m(l-1) + 2n(m+2l) - 2(l + [\frac{l+1}{2}]) \qquad \textbf{(2b)}$$

$$z = 2l \qquad \textbf{(2c)}$$

$[\frac{l+1}{2}]$ denotes an integer division such as [3/2] = 1. The definition of the indices *l,m,n* can be seen from Figure 1. *m* is parallel to <001> while *l* and *n* are parallel to <110>. The boundaries of the fragments consist of four (110) and two (001) surfaces.

COMPUTATIONAL PROCEDURE

The **E**xtended **H**ückel **M**olecular **O**rbital method (EHMO) as implemented in INPUTC/ICONC [23] was used for the calculations. This code is based on the program ICON8 [24] but has a variety of new features implemented. Concerning this paper, two modifications of the initial theory are worth mentioning. First a two-body repulsive electrostatic interaction term as was initially proposed in [25] and further developed and generalised in [26] is employed. This allows for the calculation of reasonable geometries by EHMO. Furthermore a distance dependent Hückel constant [26].

$$K(r) = 1 + \kappa \, exp(-\delta(r - d_0)), \qquad (3)$$

is implemented. κ and δ are empirical parameters, d_0 denotes the sum of the orbital radii of the involved atomic orbitals and r is the distance between the centers. This modification significantly improves the quality of the equilibrium geometries obtained by this method. Specific values for κ and δ covering a wide range of similar compounds are easily found [27]. At the equilibrium geometry, where $r \approx d_0$ the distance dependent Hückel constant coincides with the standard Hückel constant.

$$K(r = d_0) = 1 + \kappa. \qquad (4)$$

Single-ζ slater-type wave functions [28] were used for C, H, and O, while double-ζ functions [16] were used for Ti. The wave functions in [16] are slightly more diffuse than the ones used in [15] thus reproducing the experimental Ti-O bond lengths with a more reasonable value of κ. The final parameters used for the calculations are listed in Table 1. In some cases, a charge iteration procedure was applied using parameters published in [29,30] and using the H_{ii}'s in Table 1 as starting values. The coulomb integrals H_{ii} of Ti, O and H were previously determined by charge iteration at the uncharged, hypothetical complex $Ti(OH)_4$ of T_d symmetry. The more obvious choice of octahedral $Ti(OH)_6^{2-}$ leads to a wrong result due to its negative charge. The resulting values are similar to those used in previous studies on rutile [15,16]. The value of κ in the distance dependent Hückel constant was chosen to reproduce the Ti-O bond length in $Ti(OH)_6^{2-}$ while δ was left at its default value of 0.35.

To keep the results for the various adsorption geometries comparable no charge iteration at CO_2 was performed. However the H_{ii} for CO_2 were previously

Table 1
Slater exponents ζ_i and Coulomb integrals H_{ii} of the rutile part used in the calculations. $1+\kappa = 1.6$, $\delta = 0.35$. The starred oxygen H_{ii}'s were used in CO_2 where $1+\kappa = 2.0$.

Element	Orbital	ζ_i (c_i)	H_{ii} (eV)
Ti	**4s**	**1.5**	-9.72
	4p	**1.5**	-5.46
	3d	4.55 (0.42061)	-11.12
		1.40 (0.78391)	
O	**2s**	2.575	-28.80
			-29.89*
	2p	2.275	-12.14
			-13.81*
H	**1s**	**1.3**	-15.82
C	**2s**	1.71	-23.39
	2p	1.625	-13.99

determined by charge iteration at the free CO_2 molecule in its equilibrium geometry ($r_e = 1.17 \sim$ Å). They are indicated with a star in Table 1. A Mulliken population analysis was performed yielding quantities such as net charges, reduced overlap populations, . . . **D**ensity **o**f **S**tates (DOS) were calculated by convolution of the weighted energy spectrum with a gaussian of 0.2 eV width. For the total DOS each energy level has a weight $w_i = 2.0$ while for the DOS of an individual center j each level has a weight $w_{ij} = R_{ij}$. R_{ij} denotes the reduced charge matrix element of center j and level i. These weight factors ensure a proper normalisation. To visualise the results of the calculations ICON_UTILS [31] together with GEOMVIEW [32] was used to analyse and visualise the EHMO output.

RESULTS AND DISCUSSION

Small Rutile Fragments

A series of small fully hydroxylated TiO_2 fragments with rutile structure was calculated to test the parameters and the general quality of the calculations. The results are summarised in Table 2. In all cases the Ti-OH bonds were treated the same as their bulk Ti-O counterparts. This means that they were treated as belonging to the "long" or "short" set depending on their position within a TiO_6 octahedron. The O-H bonds were however kept fixed at 0.95 Å, the optimised value

Table 2
Summarized results of small rutile fragments.

l, *m*, *n*	E_{gap} [eV]	r_{Ti-O} [Å] equatorial/axial	α_{O-Ti-O}
1,1,1	2.29	1.93/1.93	90.0
1,2,1	2.01	1.84/1.99	87.5
2,1,2	1.79	1.95/1.98	90.5
2,2,2	1.67	1.92/2.02	90.0
2,3,2	1.59	1.88/2.06	89.5
3,1,2	1.76	1.98/1.96	91.0
3,2,2	1.61	1.92/2.00	90.5
3,3,2	1.55	1.92/2.04	90.0
$\infty,\infty,\infty^{\dagger}$	3.1	1.982/1.947	81.12

†Experimental bulk values from [33].

in $Ti(OH)_6^{2-}$.

While keeping the angle α_{O-Ti-O} at the experimental value of 81.12°, the two axial and the four equatorial Ti-O bonds (r_{Ti-O}) were optimised independently. With a suitable value of κ and δ the calculated bond lengths are in close agreement with the experimental values of 1.982 Å (axial) and 1.947 Å (equatorial). However, instead of octahedra with slightly longer axial Ti-O bonds as found experimentally in bulk rutile, an exactly opposite distortion with short axial bonds is found. The same discrepancy was described in an earlier study [15]. The deviation of the calculated distortion increases with increasing size of the fragment while the average Ti-O bond lengths remains in close agreement with the experimental values.

α_{O-Ti-O} was optimised while keeping the values for r_{Ti-O} at the experimental values of 1.982 Å (axial) and 1.947 Å (equatorial). Values close to 90° were generally obtained. These values deviate considerably from the experimental value of 81.12°. There is no clear trend visible for α_{O-Ti-O} for increasing fragment size. A too large α_{O-Ti-O} originates either from a too strong repulsion of the two oxygen centers facing each other on the shared edge of two TiO_6 octahedra (see Figure 6) or a too weak repulsion of the two Ti atoms sitting on each side of the edge. The fact that κ had to be reduced to a value of 0.6 to avoid unreasonably short Ti-O bonds seems to indicate that the wave functions for Ti are probably not diffuse enough, thus underestimating the Ti-Ti interaction. This would favour the second explanation for the overestimation of α_{O-Ti-O}.

At the calculated equilibrium geometries band gap energies E_{gap} were obtained. The values are generally smaller than the experimental value of 3.1 eV [33]. A strong dependence of E_{gap} on the size of the fragments is also observed. This is an manifestation of the quantum size effect (see for example [34]) predicting an increase of band gap energy for small crystallites as compared to the bulk

semiconductor.

As an example for the calculations of small rutile clusters the 3,3,2 fragment $[(TiO_2)_{31}(OH)_{32}]^{32-} \bullet 6H_2O$ has been selected. The DOS of the 175 atom fragment is shown in Figure 2. The **h**ighest **o**ccupied **m**olecular **o**rbital (HOMO) is found at -12.0 eV while the **l**owest **u**noccupied **m**olecular **o**rbital (LUMO) is at -10.5 eV. This leads to a bandgap energy E_{gap} of about 1.5 eV that is off the experimental value by a factor of two. The total DOS can be decomposed into parts associated with the different ions in the cluster. The associated partial DOS of the Ti^{4+} ions, the O^{2-} ions and the surface hydroxyl groups are also indicated in Figure 2.

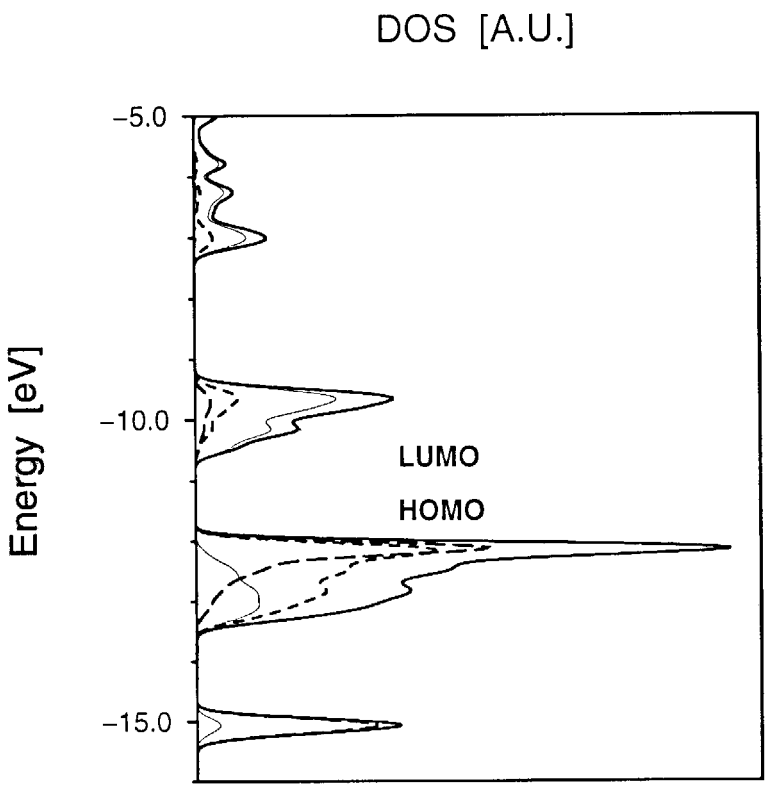

Figure 2. Density of states of the 3,3,2 fragment $[(TiO_2)_{31}(OH)_{32}]^{32-} \bullet 6H_2O$. Thick solid: total DOS; thin solid: localized on Ti; short dashed: localized on O; long dashed: localized on OH.

The orbitals giving rise to the different bands can be classified according to the local symmetry of the Ti atom (O_h is chosen over D_{4h} for simplicity reasons) and according to the type of bonding characteristic. This leads to the following interpretation of the part of the DOS shown in Figure 2. Centered around -5 eV lies a broad band of levels of local E_g symmetry that originate from $d^*_{z^2}$ and

$d^*_{x^2-y^2}$. They are mainly centered on the Ti^{4+} ions and are of Ti-O* nature. Below at -10 eV lies the conduction band. It consists of orbitals of local T_{2g} symmetry. They mainly consist of d^*_{xz}, d^*_{yz} and d^*_{xy} again with only a slight oxygen contribution. They are classified as Ti-O*. The main contributions to the valence band at about -12 eV arise from oxygen atoms. At the top of the valence band, crammed into a small energy interval, we find oxygen lone pair levels that are localised on the surface hydroxyl groups. They are followed by levels that are interpreted as bulk oxygen lone pairs generally of local T_{1g} symmetry. At the bottom of the valence band Ti-O bonding orbitals most with local T_{2g} symmetry are found. Finally O-H bonding orbitals are found at -15 eV. They show also a small contribution from titanium centers. Ti-O bonding orbitals with local E_g symmetry are situated at much lower energy. From Figure 2 one readily identifies the well known "T_{2g} above E_g" picture of the splitting of *d*-orbitals in O_h symmetry. Thus EHMO predicts rutile to have a forbidden band gap transition of $T_{2g} \leftarrow T_{1g}$ type. This result is in qualitative agreement with the experimental band structure of rutile [33] as well as with calculated band structures [35,36]. Interestingly there still exists the discussion whether the transition is direct or not [33]. A didactically very nice description of a EHMO band structure calculation of rutile, that shows the same behavior, can be found in [35].

In Figure 3 the net charges on the centers of the 3,3,2 fragment resulting from a Mulliken population analysis are presented. To simplify the picture only one eighth of the cluster is shown. Its boundaries are indicated as a box. The central Ti^{4+} ion is situated at the lower left of the figure facing the observer. The *m* direction

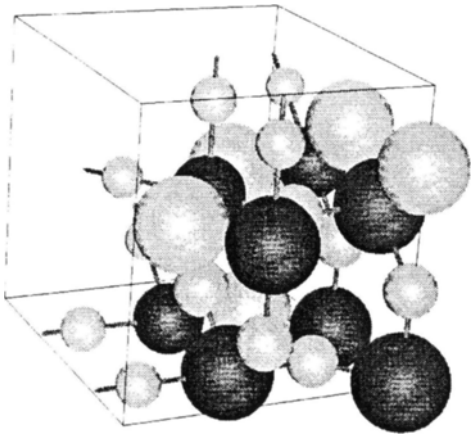

Figure 3. Net charges on the $[(TiO_2)_{31}(OH)_{32}]^{32-} \cdot 6H_2O$ cluster (3,3,2 fragment). The diameter of the spheres is proportional to the charge on a center. Light: positive charge, dark: negative charge. Only one octant of the fragment is shown.

goes to the right, while *l* and *n* directions go up and into the paper plane respectively. The radii of the indicated spheres are proportional to the charge attributed to the center. Charges smaller than ±0.1 electrons per center are omitted. Therefore no charges are indicated at the hydrogen atoms. The charge on the oxygen ions is generally about -0.5 electrons. The surface Ti-O-Ti bridging oxygens are charged almost twice as much. They thus represent Lewis base centers. Titanium centers exhibit a charge of about +1 electron. Titanium centers residing closer to the surface exhibit a slightly lower charge. The more they are coordinated by hydroxyl groups the lower is their charge.

The 3,3,2 fragment $[(TiO_2)_{31}(OH)_{32}]^{32-} \bullet 6H_2O$ is the smallest fragment that contains a TiO_6 octahedron that is coordinated exclusively by further TiO_6 octahedra. It is therefore the smallest fragment exhibiting a bulk titanium atom. In order to test the coulomb integrals H_{ii} used in the calculations, charge iteration was performed on the central Ti^{4+} ion in this fragments. The obtained values deviate only marginally from the values in Table 1 thus confirming the initial choice.

CO_2 Adsorption

Having established a feeling for the quality that can be expected from the EHMO calculations, we now proceed to describe the adsorption of a CO_2 molecule on the surface of a rutile crystallite. Oxide surfaces such as rutile show Lewis base sites (oxygen lone pairs) as well as Lewis acid sites (low coordinated surface titanium ions). This allows for several different adsorption geometries of carbon dioxide at a rutile. The ones that will now be treated in more detail are schematically indicated in Figure 4. They are very similar to the ones proposed in [37,38] to interpret FTIR spectra of CO_2 adsorbed on rutile. In this Figure 4 the rutile crystallite is indicated by a shaded rectangle and only the coordinating centers are indicated. Thus surface hydroxyls are not indicated. The actual model used for the rutile parte is shown in Figure 6. In situation *i*, *ii* and *iii* of Figure 4 CO_2 acts as a Lewis base while in situation *iv* it acts as a Lewis acid. To model situation *i* and *ii* $Ti(OH)_5^-$, a quadratic pyramid of C_{4v} symmetry was chosen to represent the rutile surface. For situation *iii* and *iv* $[(TiO_2)_2(OH)_2]^{2-} \bullet 2H_2O$ and $[(TiO_2)_2(OH)_4]^{4-} \bullet 2H_2O$ were chosen respectively. They all represent a minimal model of the rutile part and were chosen solely in favor of faster computations. In the rutile part the geometry was kept fixed at its experimental value.

CO_2 as Lewis Base: Situations i, ii and iii. An energy hypersurface was calculated for the system $Ti(OH)_5^-$-OCO representing situation *i* in Figure 4 by independently varying the Ti-OCO and the central TiO-CO bond length while keeping the

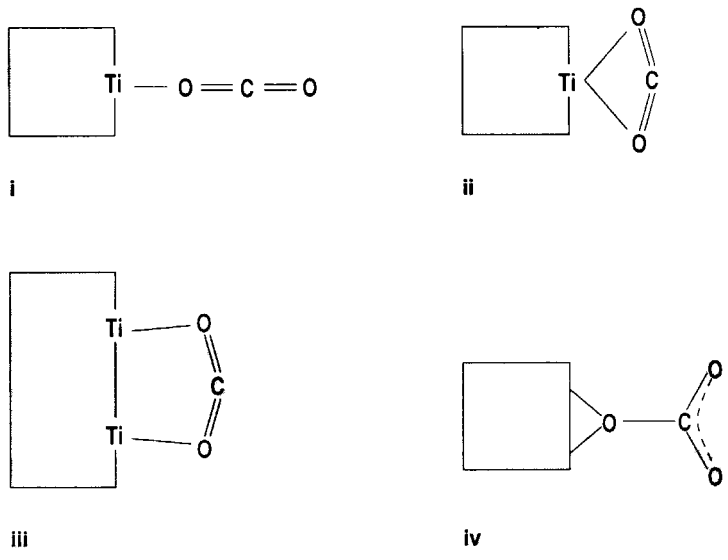

Figure 4. Different adsorption sites and geometries for CO_2 at rutile. *i* and *ii* were modeled by $Ti(OH)_5^-$, *iii* by $[(TiO_2)_2(OH)_2]^{2-} \bullet 2H_2O$ and *iv* by $[(TiO_2)_2(OH)_4]^{4-} \bullet 2H_2O$.

geometry of $Ti(OH)_5^-$ constant. The terminal C-O bond was also kept constant at 1.17 Å, the equilibrium bond length of the free carbon dioxide molecule. A minimum on the energy hypersurface was found at $r_{Ti\text{-}OCO} = 2.0$ Å and $r_{TiO\text{-}CO} = 1.15$ Å with a stabilisation energy of 0.81 eV. The calculated equilibrium geometry corresponds closely to an undisturbed CO_2 molecule at a distance of 2.0 Å away from the Ti center. This distance coincides within the accuracy of the calculation with the average Ti-O bond length earlier found for various rutile fragments. The small stabilization energy together with the almost undisturbed CO_2 molecule at the distance of an average Ti-O bond are indications that a weak adsorption of CO_2 at rutile is to be expected.

After having established the equilibrium geometry of the model system $Ti(OH)_5^-$-OCO the interaction between the two parts is now analyzed in more details. In Figure 5, a correlation diagram describing the main interactions is shown. There are only minor interactions of occupied levels that contribute to the adsorption of carbon dioxide. The most prominent interaction involves the LUMO of CO_2 (π^* with E symmetry in D_{4v}) and the LUMO of $Ti(OH)_5^-$ (d^*_{xz}, d^*_{yz}). As these are unoccupied levels they will not contribute to any bonding interaction between CO_2 and rutile. The adsorption of CO_2 at $Ti(OH)_5^-$ causes a minimal charge transfer of about 0.2 electrons from CO_2 onto $Ti(OH)_5^-$. A reduced overlap population of 0.2251 between Ti and O is found supporting the interpretation of a weak interaction of CO_2 with rutile.

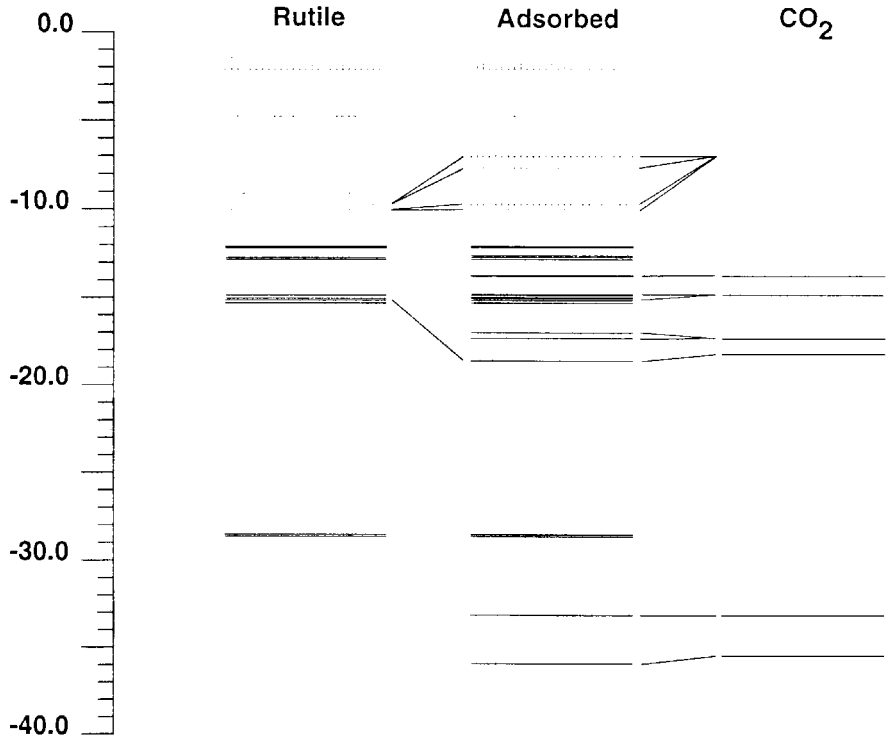

Figure 5. Correlation diagram of CO_2 interaction with $Ti(OH)_5^-$ for CO_2 perpendicular to the surface. Unoccupied levels are represented by dotted lines.

If the same calculation is performed with charge iteration at CO_2 the outcome is quite different. The H_{ii}'s of the carbon dioxide molecule are lowered considerably and therefore the interaction of π^* orbital with the $d^*_{xz,yz}$ is enhanced to an extent that the bonding combination is stabilized so strongly that it becomes occupied. This leads to a charge transfer of two electrons from the the $Ti(OH)_5^-$ part to the CO_2 molecule. This would imply that TiO_2 is able to reduce CO_2, a situation that is not observed experimentally. This is however a well known problem that occurs when charge iteration within the EHMO framework is applied to weakly bound systems.

To find out whether an additional stabilization of CO_2 bound to $Ti(OH)_5^-$ could be achieved by allowing for the interaction of the carbon atom with a oxygen atom of a hydroxyl group at $Ti(OH)_5^-$, both angles ϕ and ψ (see Figure 6) were independently varied. A rather shallow minimum is found for both angles being 180°. This does suggest that CO_2 remains linear and is only coordinated to the titanium center. To allow for a possible interaction of the carbon atom with a

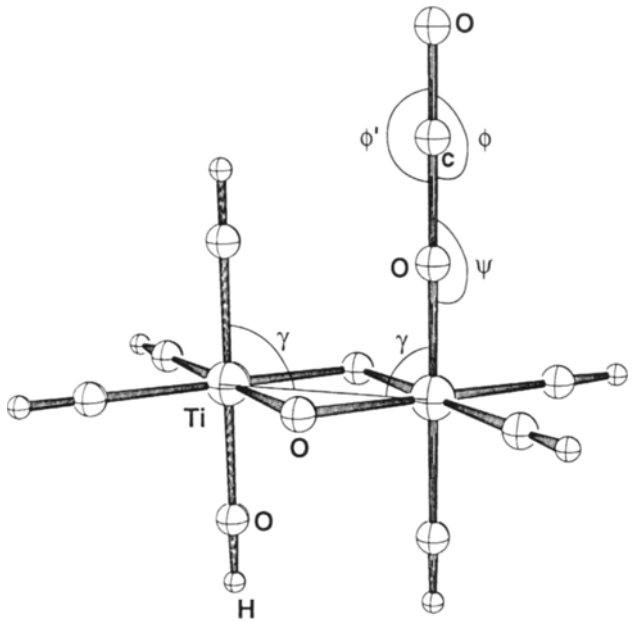

Figure 6. Definition of angles ϕ, ψ and γ in $Ti(OH)_5^-$-OCO and $[(TiO_2)_2(OH)_2O]^- \bullet 2H_2O$-OCO [39].

hydroxyl group of a neighboring TiO_6 octahedron, $[(TiO_2)_2(OH)_2O]^- \bullet 2H_2O$, a 1,2,1 fragment consisting of two edge-shearing $Ti(OH)_6$ octahedra where one octahedron is only fivefold coordinated and a neighboring hydroxyl group on the other octahedra is replaced by an O^{2-} ion, was chosen. γ and ϕ′ as defined in Figure 6 were varied, but again no deviation from the linear geometry of CO_2 was found. This is in contrast to [37] who also proposes an oxygen-coordinated bent CO_2 species.

Situation *ii* of Figure 4 models the possibility of carbon dioxide adsorbing parallel to the surface on a single Ti^{4+} center. This corresponds to situation IV and VI of [37]. $Ti(OH)_5^-$ was chosen as model for the rutile surface. CO_2 was turned by 45° around the C_4 axis of $Ti(OH)_5^-$ to minimize the repulsion between the hydroxyl groups and the oxygen atoms of CO_2. The resulting complex has C_{2v} symmetry. The distance $r_{Ti\text{-}C}$ and the bending angle ϕ at CO_2 were varied independently. The geometry of $Ti(OH)_5^-$ and the bond length in CO_2 were both kept constant at their respective equilibrium values. No charge iteration was performed in this calculation. A minimum was found for $r_{Ti\text{-}C}$ = 1.8 Å and ϕ = 160° with a slightly smaller stabilization energy (0.65 eV) than for the linearly coordinated case *i* discussed above. The carbon dioxide molecule is slightly bent towards $Ti(OH)_5^-$ at the minimum of the energy hypersurface thus acting as a bidentate ligand.

Therefore a chelating structure seems more stable than one where a Ti-C bond has been formed. In Figure 7, a correlation diagram at the minimum of the energy hypersurface is shown. The splitting of the degenerate energy level of CO_2 upon adsorption due to symmetry reduction from $D_{\infty h} \rightarrow C_{2v}$ is clearly visible. Most of the correlation diagram in Figure 7 can be interpreted in terms of a Walsh diagram for the bending motion of carbon dioxide. The only strong interaction between carbon dioxide and $Ti(OH)_5^-$ is found in the non-bonding regime between the A_1 component of the π^* LUMO of CO_2 and the $d^*_{z^2}$ and the $d^*_{xz,yz}$ orbitals of $Ti(OH)_5^-$.

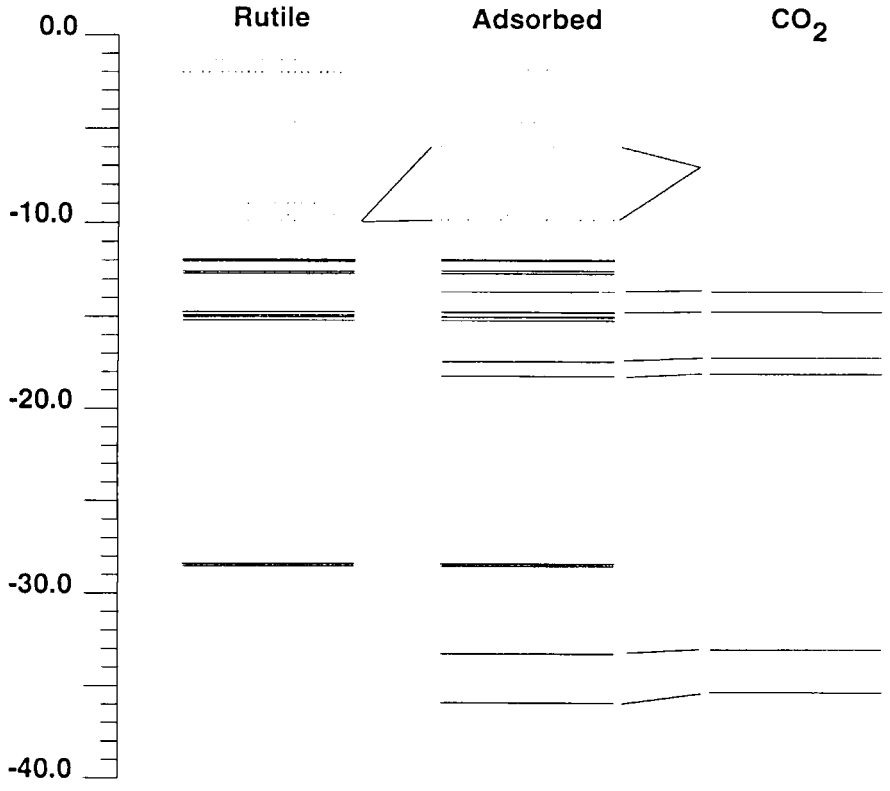

Figure 7. Correlation diagram of CO_2 interaction with $Ti(OH)_5^-$ for CO_2 parallel to the surface. Interaction with one Ti^{4+} center. Unoccupied levels are represented by dotted lines.

A marginal charge transfer of 0.1 electrons from $Ti(OH)_5^-$ onto carbon dioxide was found from a Mulliken population analysis. This values is smaller and of opposite sign than in the case of linear coordination of CO_2 to $Ti(OH)_5^-$. The reduced overlap population between the carbon atom and the Ti atom is found to be -0.25 while the one between the oxygen atom of CO_2 and the Ti atom is -0.07. This

does not confirm the hypothesis that CO_2 can act as a chelating ligand at the rutile surface. The binding of carbon dioxide to $Ti(OH)_5^-$ is therefore very weak and mostly due to the stabilization occurring in CO_2 caused by the bending of the molecule and the interaction of the CO_2 oxygen atoms with σ-bonding orbitals of the hydroxyl groups. As seen from a Walsh diagram, only the neutral CO_2 can be expected to be linear. Adding or removing charge from the molecule will favour a slightly bent C_{2v} configuration. As discussed above there is a small charge transfer from CO_2 to the Ti^{4+} center thus a slightly bent configuration can be expected. If the calculation is performed with charge iteration at carbon dioxide no adsorption at all is found. To summarize, the net stabilization in this case is only about 75% of case *i*. This is mostly due to the weak interaction of CO_2 with the hydroxyl groups leading to a small charge transfer and a bent CO_2. The fact that upon charge iteration at CO_2 no bound complex could be found, shows that the adsorption in this geometry, if occuring at all, must be very weak.

Comparing the Ti-Ti distance of 2.96 Å in the 1,2,1 fragment $[(TiO_2)_2(OH)_2]^{2-} \bullet 2H_2O$ with the O-O distance of 2.34 Å in carbon dioxide it can be imagined that CO_2 binds to two neighboring Ti^{4+} sites. This corresponds to situation *iii* in Figure 4 where a Ti-O-C-O-Ti five-ring is formed. The geometry of the rutile part and the C-O bonds of carbon dioxide were kept fixed at their equilibrium geometries while the distance *d* between the carbon atom and the rutile surface and the bending angle ϕ at CO_2 were varied. A minimum on the energy hypersurface was found at $d = 2.3$ Å and $\phi = 155°$, with CO_2 bent towards the surface. This corresponds to a Ti-O distance of 2.07 Å. Figure 8 shows a correlation diagram describing the main interactions at the minimum energy. The situation is very similar to the one already reported for situation *i* (see Figure 5). This has to be expected as both situations basically comprise an interaction of a oxygen center of CO_2 with a fivefold coordinated Ti^{4+} ion. Thus, again the interaction of the d-orbitals belonging to local E_g symmetry with the σ_u^+ orbital dominates. The corresponding molecular orbital is depicted in Figure 9. Because two Ti-O interactions are involved in situation *iii* the stabilization of the energy level at 18.98 eV is stronger. This results in a net stabilization energy of 1.45 eV which is about twice as much as in situation *i*. A reduced overlap population of 0.10 is found between the Ti center and the coordinating oxygen center of CO_2. In this geometry a charge transfer of 0.22 electrons from the carbon dioxide molecule to the rutile is found.

CO_2 as Lewis Acid: Situation iv. We now discuss situation *iv* of Figure 4 as an example of CO_2 acting as an Lewis acid. The rutile part was modeled by $[(TiO_2)_2(OH)_4]^{4-} \bullet 2H_2O$. In Figure 4 CO_2 interacts with the oxygen atom belonging to an Ti-O-Ti bridge at the surface of the crystallite. The same general conclusion

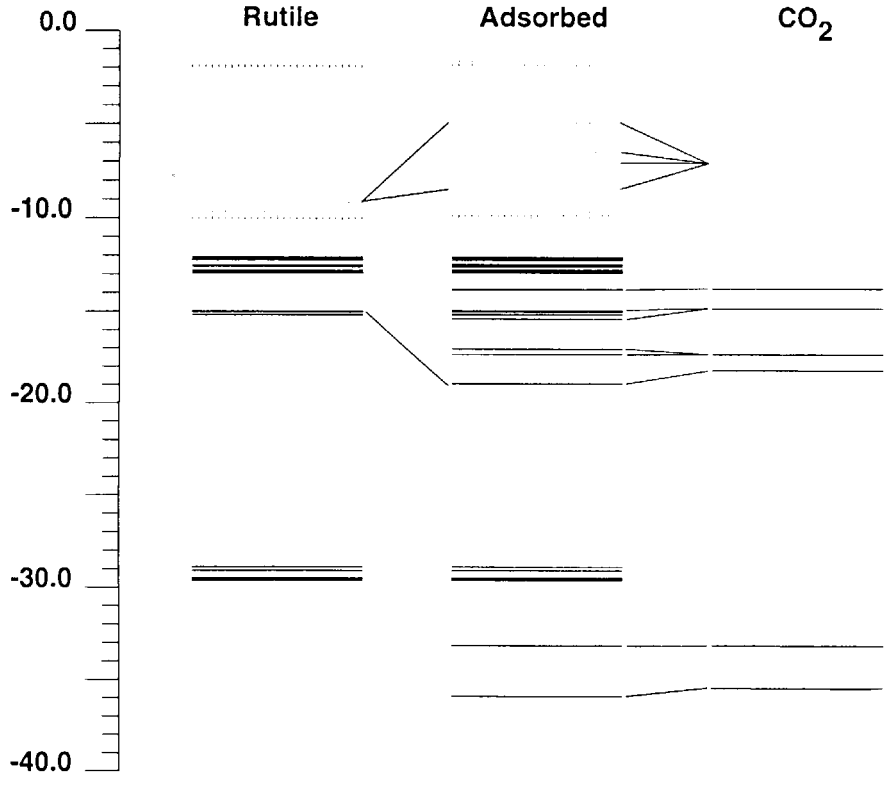

Figure 8. Correlation diagram of CO_2 interaction with $[(TiO_2)_2(OH)_2]^{2-} \bullet 2H_2O$. Interaction with two Ti^{4+} centers. Unoccupied levels are represented by dotted lines.

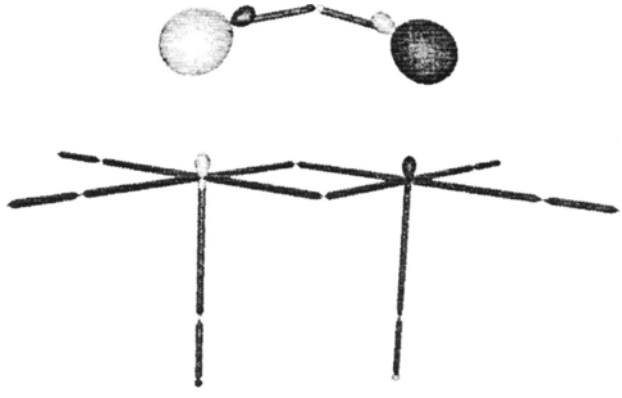

Figure 9. Molecular orbital showing the bonding interaction of Σ_u^+ with the E_g d-orbitals of the Ti^{4+} center. This orbital is mainly responsible for a bonding interaction.

however can be drawn if one considers the interaction of CO_2 with a terminal oxygen atom in the rutile structure instead. The carbon dioxide molecule was rotated 90° out of the Ti-O-Ti plane to minimize repulsion by neighboring hydroxyl groups. The energy hypersurface was determined by independently varying the distance $d_{C\text{-}O\ bridge}$ and the bond angle ϕ at CO_2. For the rutile part and the C-O bond length experimental values were used and kept fixed. Additionally a value $1+\kappa = 2.0$ of the Hückel constant was used for the C-O_{bridge} interaction to avoid an unreasonable length of the C-O_{bridge} bond. An energy minimum on the hypersurface was found for $d_{C\text{-}O\ bridge}$ = 1.31 Å and ϕ = 130°. Comparing these values to the one of the free carbonate ion CO_3^{2-} (r = 1.30 Å and ϕ = 120°) obtained by EHMO one realizes that this adsorption geometry corresponds to a carbonate like species. This interpretation is furthermore supported by the transfer of 1.07 electrons from the rutile to the adsorbed molecule and the reduced overlap population of 0.83 between the bridging oxygen and the carbon atom. The interpretation of a carbonate like species is also supported by a comparison of the reduced overlap population within the CO_2 molecule (1.07) with the one of the O_{bridge} (0.83).

The correlation diagram as obtained at the energy minimum is reported in Figure 10 to interpret the binding situation. Part of the diagram can again be

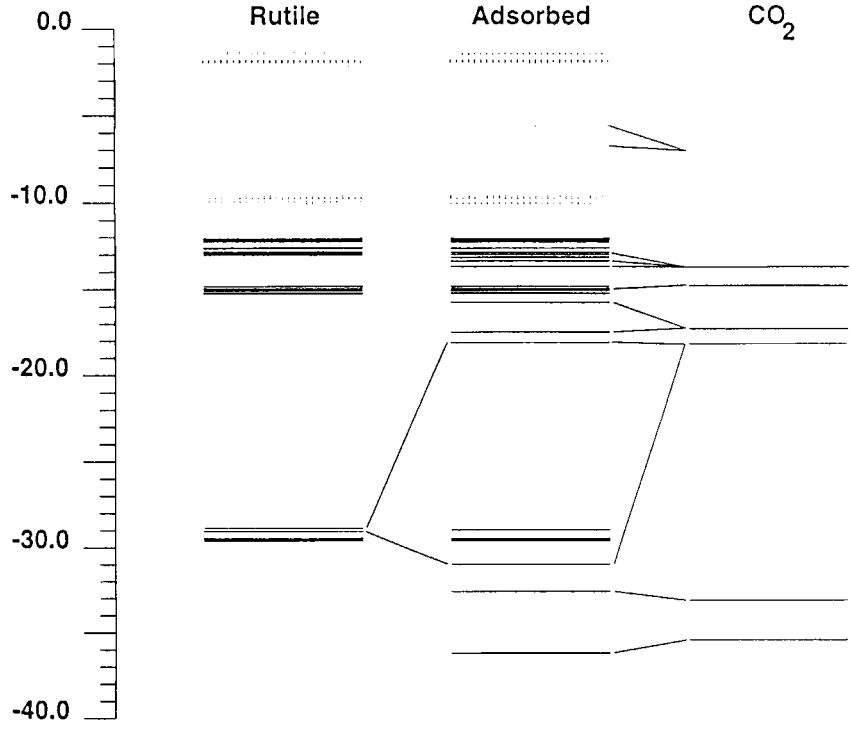

Figure 10. Correlation diagram of carbonate-like CO_2. Unoccupied levels are represented by dotted lines.

explained by the bending of the molecule upon adsorption. They compensate each other quite well thus they do not contribute to the bending. However two additional strong interactions responsible for the binding are identified. The corresponding MO's are illustrated in Figure 11. We see that two Σ_g^+ orbitals of CO_2 interact strongly with the rutile bridging atom. These two interactions are therefore responsible for the binding of CO_2 to the bridging oxygen atom.

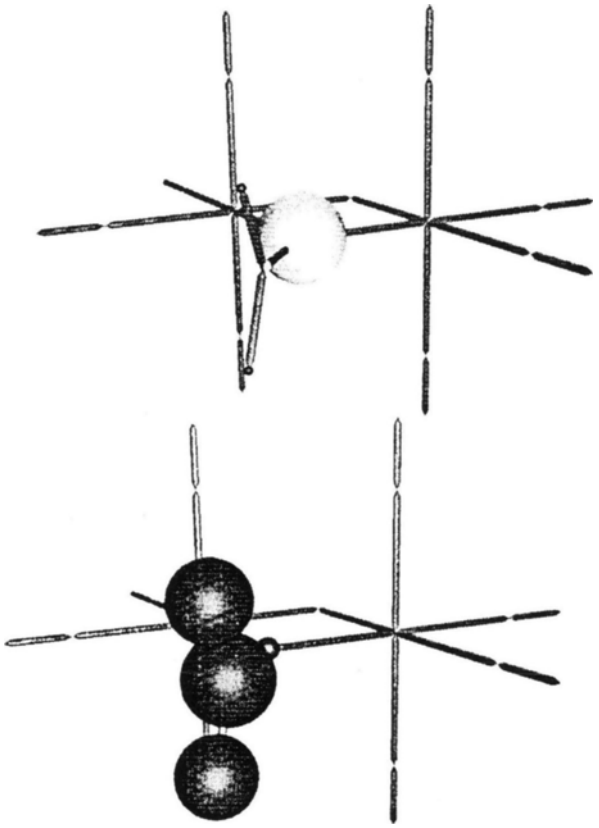

Figure 11. Molecular orbitals mainly responsible for the stability of carbonate-like CO_2.

CONCLUSIONS

The EHMO method as introduced in Section II is suitable to describe qualitatively the bulk equilibrium geometry and the electronic structure of rutile. The ordering and the type of the bands agree quite well with experimental and theoretical data and the experimental bond lengths were reproduced with astonishing precision. The

distortion of the TiO_6 octahedra, however, was found opposite to the experimental one. Bond angles could not be reproduced well. The absolute energies obtained do also not agree with the experimental values which is a well known deficiency of the method. Furthermore it was shown that CO_2 adsorbs at Lewis acid as well as Lewis base sites. For Lewis acid sites (fivefold coordinated surface Ti^{4+} ions), an adsorption geometry with CO_2 perpendicular to the surface or the adsorption at two neighboring Ti^{4+} sites is stable. The possibility of carbon dioxide acting as a bidentate ligand or adsorbing by the formation of a Ti-C bond is not stable. The formation of a carbonate-like species is identified upon the adsorption of CO_2 at a surface oxygen ion. In this case carbon dioxide acts as a Lewis acid.

Acknowledgements
This work has been supported by the Swiss Federal Office of Energy.

REFERENCES

1. M. Anpo and Y. Kubokawa, *Res. Chem. Intermed.* **8** 105 (1987).
2. M. Anpo, *Res. Chem. Intermed.* **11**, 67 (1989).
3. M. Anpo *et al.*, *Bull. Chem. Soc. Jpn.* **64**, 543 (1991).
4. N. Serpone, R. Terzian, D. Lawless, and J.-M. Herrmann, *Adv. Electron Transfer Chemistry* **3**, 33 (1993).
5. A.L. Linsebigler, G. Lu, and J.T. Yates, Jr., *Chem. Rev.* **95**, 735 (1995).
6. A. Fujishima and K. Honda, *Nature* **238**, 37 (1972).
7. A.J. Bard and M.A. Fox, *Acc. Chem. Res.* **28**, 141 (1995).
8. M. Anpo and K. Chiba, *J. Mol. Catal.* **74**, 207 (1992).
9. K. Ogura, M. Kawano, J. Yano, and Y. Sakata, *J. Photochem. Photobiol. A: Chem.* **66**, 91 (1992).
10. H. Yamashita, N. Kamada, H. He, K. Tanaka, and M. Anpo, *Chem. Lett.* 855 (1994).
11. H. Yamashita *et al.*, *Energy Convers. Mgmt* **36**, 617 (1995).
12. F. Saladin, L. Forss, and I. Kamber, *J. Chem. Soc., Chem. Commun.* 533 (1995).
13. F. Saladin, A. Meier, and I. Kamber, *Rev. Sci. Instrum.* **67**, 2406 (1996).
14. T. Bredow and K. Jug, *Chem. Phys. Lett.* **223**, 89 (1994).
15. J. Burdett, *Inorg. Chem.* **24**, 2244 (1985).
16. C.-R. Wang and Y.-S. Xu, *Surf. Sci.* **219**, L537 (1989).
17. B. Viswanathan and T. Lakshmi, *Indian J. Chem.* **A 32**, 937 (1993).
18. T. Bredow and K. Jug, *Surf. Sci.* **327**, 398 (1995).
19. H. Takaba *et al.*, *Energy Convers. Mgmt* **36**, 439 (1995).
20. D.C. Sayle, R.A. Catlow, M.-A. Perrin, and P. Nortier, *J. Phys. Chem. Solids* **56**, 799 (1995).
21. V.E. Henrich and P.A. Cox, *The Surface Science of Metal Oxides* , Cambridge University Press, UK, 1994.
22. R.J.D. Miller *et al.*, *Surface Electron Transfer Processes,* VCH Publishers, New York, 1995.
23. G. Calzaferri and M. Brändle, *QCMP Bull.* 12 (1992), update May 1993.
24. J. Howell *et al.*, *ICON8 quantum chemistry program performing extended-Hückel*

calculation, QCPE No. 344, 1978.
25. A.B. Anderson and R. Hoffmann, *J. Phys. Chem.* **60**, 4271 (1974).
26. G. Calzaferri, L. Forss, and I. Kamber, *J. Phys. Chem.* **93**, 5366 (1989).
27 F. Savary, J. Weber, and G. Calzaferri, *J. Phys. Chem. 97*, 3722 (1993).
28. N. Fitzpatrick and G. Murphy, *Inorg. Chem. Acta* **87**, 41 (1984).
29. H. Basch, A. Viste, and H. Gray, *Theoret. Chim. Acta (Berl.)* **3**, 458 (1965).
30. H. Basch and H. Gray, *Theoret. Chim. Acta (Berl.)* **4**, 367 (1966).
31. I. Kamber, *ICON-UTILS -- A Collection of Utilities to Visualize the Output of EHMO Calculations*, 1996.
32. *Geomview, Version 1.5*, Software Development Group, Geometry Center, Minneapolis, US, 1994, availabe for free at geom.umn.edu.
33. Goodenough and Hamnett, *Landolt-Börnstein*, New Series III 17g.
34. Y. Wang. In: *Photophysical and Photochemical Processes of Semiconductor Nanoclusters*, Vol. 19 of *Adv. Photochem.*, D.C. Neckers, D.H. Volman, and G. von Brünau (Eds.), John Wiley & Sons, Inc., New York, 1995, pp. 179-234.
35. R. Hoffmann, *Solids and Surfaces: A Chemist's View of Bonding in Extended Structures*, VCH Verlagsgesellschaft mbH, Weinheim, 1988.
36. B. Poumellec, P.. Durham, and G.Y. Guo, *J. Phys.: Condens. Matter.* **3**, 8195 (1993).
37. G. Ramis, G. Busca, and V. Lorenzelli, *Mater. Chem. Phys.* **29**, 425 (1991).
38. J. Raskó and F. Solymosi, *J. Phys. Chem.* **98**, 7147 (1994).
39. M.N. Burnett and C.K. Johnson, *ORTEP-III: Oak Ridge Thermal Ellipsoid Plot Program for Crystal Structure Illustrations*, 1996, Oak Ridge National Laboratory Report ORNL-6895.